# Examining the Thermal Properties of 3D Printed Models Produced by Fused Deposition Modeling and Stereolithography

Shu-An Hsieh and Jared L. Anderson\*

Department of Chemistry, Iowa State University, Ames, Iowa, USA

#### Abstract

**Purpose** – This work studies the mass loss of 3D printed materials at high temperatures. A preconcentration and analysis technique, static headspace gas chromatography-mass spectrometry (SHS-GC-MS), is demonstrated for the analysis of volatile compounds liberated from fused deposition modeling (FDM) and stereolithography (SLA) 3D printed models under elevated temperatures.

**Design/methodology/approach** – A total of seven commercial 3D printing materials were tested using the SHS-GC-MS approach. The printed model mass and mass loss were examined as a function of FDM printing parameters including printcore temperature, model size, and printing speed, and the use of SLA post-processing procedures. A high temperature resin was used to demonstrate that thermal degradation products can be identified when the model is incubated under high temperatures.

**Finding** – At higher printing temperatures and larger model sizes, the initial printed model mass increased and showed more significant mass loss after thermal incubation for FDM models. For models produced by SLA, the implementation of a post-processing procedure reduced the mass loss at elevated temperatures. All FDM models showed severe structural deformation when exposed to high temperatures, while SLA models remained structurally intact. Mass spectra and chromatographic retention times acquired from the high temperature resin facilitated identification of eight compounds (monomers, crosslinkers, and several photoinitiators) liberated from the resin.

**Originality/Value** – The study exploits the high sensitivity of SHS-GC-MS to identify thermal degradation products emitted from 3D printed models under elevated temperatures. The results will aid in choosing appropriate filament/resin materials and printing mechanisms for applications that require elevated temperatures.

**Keywords** Fused deposition modeling, Stereolithography, Static headspace gas chromatographymass spectrometry

Paper type research paper

## **Corresponding Author:**

Jared L. Anderson Iowa State University 1605 Gilman Hall Ames, IA 50011

Tel.: +1 515-294-8356

E-mail address: andersoj@iastate.edu

## 1. Introduction

Three-dimensional (3D) printing technologies, also known as additive manufacturing, has spurred considerable excitement and created tremendous opportunities for a number of research fields within the analytical sciences (Au *et al.*, 2016; Carvalho *et al.*, 2018; Hearn, 2017; Kalsoom *et al.*, 2018; Li *et al.*, 2020; Su *et al.*, 2015; Wang and Pumera, 2021; Weigel *et al.*, 2021; Weisgrab *et al.*, 2019). Advantages of 3D printing include rapid prototyping (Campbell *et al.*, 2012; Macdonald *et al.*, 2014), structural design customization (Srinivasan *et al.*, 2017), and low cost fabrication (Chan *et al.*, 2016; Kahl *et al.*, 2019). Various material options including plastics (Blok *et al.*, 2018; Valino *et al.*, 2019), resins (Borrello *et al.*, 2018; Guerra *et al.*, 2019; Warr *et al.*, 2020), and metals (Hong *et al.*, 2020; Wang *et al.*, 2021) provide the potential for highly versatile 3D printing in a wide range of applications. In addition, 3D printers have also been commercialized and remodeled into desktop formats (Moseng, 1992), making 3D printing technology more simple and affordable for educational (Ford and Minshall, 2019) and home-use purposes (Rayna and Striukova, 2016).

To date, a number of 3D printing mechanisms such as selective laser sintering (Awad *et al.*, 2020), selective laser melting (Hong *et al.*, 2020), and inkjet 3D printing (Basak *et al.*, 2020) have been developed. Among the 3D printing methods, fused deposition modeling (FDM) and stereolithography (SLA) are the most popular in the additive manufacturing industry. FDM, also known as fused filament fabrication, is comprised of one or several printing nozzles, a vertical movable print bed, and a material feeder. The nozzle moves above the print bed and heats to a specific temperature, causing the filament to soften. The filament(s) are then pressurized by the heated nozzle and extruded onto a print bed. After completing the first layer of printing, the print bed moves downward and the next layer begins printing on the initial layer. Once printing is

complete, the model can be simply removed from the build plate without additional postprocessing procedures (Mwema and Akinlabi, 2020). Advantages of FDM printing are its rapid
printing speed and cheap filament materials, which typically cost approximately 50 USD per spool.

SLA printers, on the other hand, employ a UV light source that polymerizes the resin in a layerby-layer fashion from the bottom of a resin tank. As opposed to FDM printing, SLA printed objects
are composed of a single resin material and are often considerably more expensive. Nevertheless,
they possess a smooth surface and are highly detailed due to the small contact area of the highlyprecise laser (Borrello *et al.*, 2018), and have a high degree of strength and rigidity since the layers
are connected by crosslinked polymers. Even though FDM printers have the ability reach a
minimum printing layer thickness of 10 micrometers, most desktop FDM printers can only achieve
a thickness of 100 micrometers, whereas commercial SLA printers can easily get down to 25
micrometers per layer without concerns of extrusion nozzle clogging. Because SLA and FDM
possess their own advantages and disadvantages, it is important for users to decide which benefits
are more suitable for their desired application.

The global SARS-CoV-19 pandemic led to the wide-spread manufacturing of 3D printed masks and respirators due to shortages in traditional personal protective equipment (Choong *et al.*, 2020). Despite the numerous aforementioned benefits of 3D printing technologies, previous studies have highlighted numerous safety concerns of 3D printed products due to strong odors that emanate from them (Chan *et al.*, 2020; Even *et al.*, 2019). Common 3D printing materials may be incompletely polymerized, leading to uncured resin being trapped inside the formed polymers and subsequent production of volatile organic compounds (VOCs) when exposed to high temperatures. Several studies have reported the emission of odor/odorless VOCs from 3D printers during the printing process (Even *et al.*, 2019; Potter *et al.*, 2019; Stephens *et al.*, 2013; Zhang *et al.*, 2019).

However, few studies have examined VOC emission from the thermal degradation of 3D printed objects under elevated temperature conditions. Wan et al. reported the use of thermogravimetric analysis to mimic the nozzle heating process and determine total VOCs (TVOCs) of 3D printed objects (Ding et al., 2019). However, the composition and identity of compounds emitted from the filaments still remains largely unknown. Bernatikova et al. evaluated ultrafine particles and VOCs from the decomposition of FDM filaments during printing (Bernatikova et al., 2021). Qualitative analysis of TVOCs released during the FDM printing process were measured by a photoionization detector equipped with a datalogger, while gas chromatography-mass spectrometry (GC-MS) coupled with thermal desorption tubes was used to analyze air samples collected from the confined 3D printing system. The setup required the construction of a confined system covering the 3D printer. Additionally, thermal desorption tubes have the disadvantage of slow sample collection and low precision, often requiring long sampling durations to acquire enough sample for analysis. Moreover, since the printing nozzle and bed are both required to heat during printing, the collected thermal decomposition products may originate from both the nozzle and model, making it challenging to identify the exact source of VOC emission. Therefore, alternative techniques that consolidate heating and sample extraction while possessing short analysis times, high sensitivity, and capability of identifying the composition of thermal decomposition and/or degradation products are needed.

Static headspace sampling (SHS) is a well-established technique for the analysis of VOCs from liquid/solid sample matrices (Alvarado and Rose, 2004; Rodinkov *et al.*, 2020). SHS involves incubation of a sample sealed in a vial within a temperature-controlled oven resulting in the release of thermal degradation/volatilization products to the headspace of a sealed vial. A sampling needle and injector is used to penetrate the septum on the sealed cap, withdraw a fraction of the gaseous

headspace, and transfer the sample to the inlet of a gas chromatograph (GC) where the analytes are separated and analyzed. Flame ionization (FID) (Badaro *et al.*, 2021) and electron capture (ECD) (Russo *et al.*, 2021) detectors can be coupled with SHS-GC analysis, but they are limited since they often do not provide information that can assist in structural elucidation of the volatile molecules. The coupling of MS with SHS-GC permits the trace analysis of volatile molecules as well as the ability to structurally characterize volatile impurities to identify odor-causing compounds (Fuller *et al.*, 2020). contaminants (Cardador and Gallego, 2017), or residual solvents in pharmaceutical products (Yarramraju *et al.*, 2007).

In this study, we demonstrate the coupling of SHS with GC-MS to analyze VOCs released directly from 3D printed objects produced by FDM and SLA and its utility for testing the thermal stability and robustness of 3D printing materials at elevated temperatures. A total of three FDM filaments and four SLA resins were chosen based on their recommended high temperature applications from the manufacturer and their thermal stability. To investigate the amount of VOCs emitted from 3D printed materials at various elevated temperatures, SHS was used for accurate control of incubation conditions allowing the mass reduction of the models to be determined. All 3D printed materials examined in this study were observed to exhibit shape deformation and/or color changes after thermal analysis at temperatures ranging from 100 °C to 240 °C. Finally, we demonstrate the potential of using GC-MS in the qualitative determination of thermal degradation/decomposition products originating from 3D printed materials using the National Institute of Standards and Technology (NIST) mass spectral library.

## 2. Experimental

## 2.1 Reagents and materials

Commercial SLA resins (clear FLGPCL04, high temperature FLHTAM02, castable wax FLCWPU01, flexible 80A FLFLGR02) were purchased from Formlabs Inc. (Somerville, MA, USA). FDM filaments (red acrylonitrile butadiene styrene (ABS), transparent copolyester+ (CPE+), transparent polycarbonate (PC)) were purchased form Dynamism Inc. (Chicago, IL, USA). HPLC grade isopropanol (99%, IPA) was purchased from Sigma-Aldrich (St. Louis, MO, USA). Headspace glass vials (10 mL), headspace caps, and a manual vial crimper were purchased from Agilent Technologies, Inc. (Santa Clare, CA, USA).

## 2.2 Methods

## 2.2.1 Production of 3D printed models

The 3D printed model used throughout this study was designed by Autodesk Inventor Professional 2021 software from Autodesk Inc. (Mill Valley, CA, USA) and had the dimensions of 5 mm x 5 mm x 5 mm (L x W x H), as shown in Figure S1. The design was saved and then sent to two software slicers, Ultimaker Cura (Geldermalsen, Netherlands) and Formlabs Preform (Somerville, MA, USA) to set up the printing parameters. FDM printing was carried out using a Ultimaker3 printer (Geldermalsen, Netherlands). The printing parameters included a layer height of 0.15 mm, printing speed of 60 mm/sec, and printing temperature of 235 °C for ABS, 270 °C for CPE+, and 280 °C for PC. SLA prints were performed on a Form3 printer (Somerville, MA, USA). The parameters included a layer height of 100 µm for the clear, high temperature, flexible 80A, and castable wax resins. FDM and SLA printing parameters were saved as 3D printer compatible files and then sent to the 3D printers. Following printing, all SLA models were washed with IPA in Form Wash obtained from Formlabs Inc. As suggested by the manufacturer, clear resin models required 10 minutes, high temperature resin models required 6 minutes, flexible 80A resin models required 20 minutes, and castable wax resin models 5 minutes of IPA wash. The clear and flexible

80A resin models required 15 and 10 minutes, respectively, of thermal and UV curing at 60 °C in Form Cure from Formlabs Inc. Models produced from the high temperature resin required conditioning at 80 °C for 120 minutes in Form Cure and additional 180 minutes at 160 °C in the vacuum oven. Castable wax resin models were fully dried by a lint-free wipe after the IPA wash and used without further curing.

# 2.2.2 Static headspace gas chromatography-mass spectrometry

The mass of printed models was initially obtained on a Mettler-Toledo microbalance (Columbus, OH, USA). An Agilent Technologies 7697A headspace sampler (HS) coupled with an Agilent Technologies 7890B gas chromatograph (GC) equipped with an Agilent Technologies 5977A mass spectrometer (MS) employing electron ionization was employed throughout this study. 3D printed models were placed into a headspace sample vial, manually sealed with headspace caps using a vial crimper, and placed on the tray of the headspace sampler vial rack. HS oven temperatures were varied from 100 °C to 240 °C in 20 °C increments and all vials were incubated at the respective temperature using an equilibrium time of 20 minutes. A 1 mL sample loop was employed in the static headspace sampler and set at 250 °C. A volume of 1.0 mL was sampled using a 30 psi vial pressure and 20 psi loop pressure. The transferline connecting the headspace sampler and GC was set at 250 °C to prevent sample condensation. A prosteel metal capillary tubing (1 meter long with 530 µm inner diameter (I.D.)) was employed as the transfer line. All chromatographic separations were carried out using a Rtx-5MS capillary column (30 m x 250  $\mu$ m I.D., d<sub>f</sub> = 0.25  $\mu$ m) from Restek (Bellefonte, PA, USA). The GC injection temperature was maintained at 250 °C with a total flow rate of 9 mL min<sup>-1</sup>, septum purge flow of 3 mL min<sup>-1</sup>, and a 5:1 split ratio. The GC inlet pressure was held at 11.639 psi to maintain a column flow rate of 1 mL min<sup>-1</sup>. Helium was used as the carrier gas for all separations. The employed GC temperature

program was as follows: initial temperature of 40 °C and held for 20 minutes, 10 °C/min ramp to 100 °C, followed by a 2 °C/min ramp to 120 °C, and a 15 °C/min ramp to 300 °C, and finally held for 15 minutes. The MS source was set at 230 °C in the EI mode with a scan range of 45-300 m/z. All chromatograms and mass spectra were acquired using MassHunter software from Agilent Technologies (Santa Clare, CA, USA). After SHS analysis, all models were removed from the headspace vials and their final mass acquired using a microbalance.

## 3. Results and discussions

# 3.1 Effect of headspace oven temperature on mass reduction of 3D printed models

In this study, four SLA resins (clear, high temperature, flexible 80A, and castable wax) and three FDM filaments (ABS, CPE+, and PC) were examined. A microbalance was used to weigh the models before and after the samples were subjected to the SHS-GC-MS system. The thermal stabilities of all prepared models were evaluated and compared by determining the mass reduction of each model after incubation at different temperatures. All models were incubated for 20 minutes in the HS oven at 100 °C, 120 °C, 140 °C, 160 °C, 180 °C, 200 °C, 220 °C, and 240 °C.

The mass reduction for each model was calculated using equation 1:

Mass reduction (%) = 
$$\frac{\text{(initial model mass-final model mass)}}{\text{initial model mass}} \times 100 \text{ (Eq. 1)}$$

where the initial mass of the sample (in grams) is measured before placing the sample in the headspace vial, and the final mass of the sample is measured upon removing the sample from the vial after HS analysis. The relationship between mass reduction and the employed headspace oven temperature is shown in Figure 1. All studied materials exhibited a mass reduction when exposed to elevated HS oven temperatures. At 240 °C, the mass reduction of SLA materials decreased in

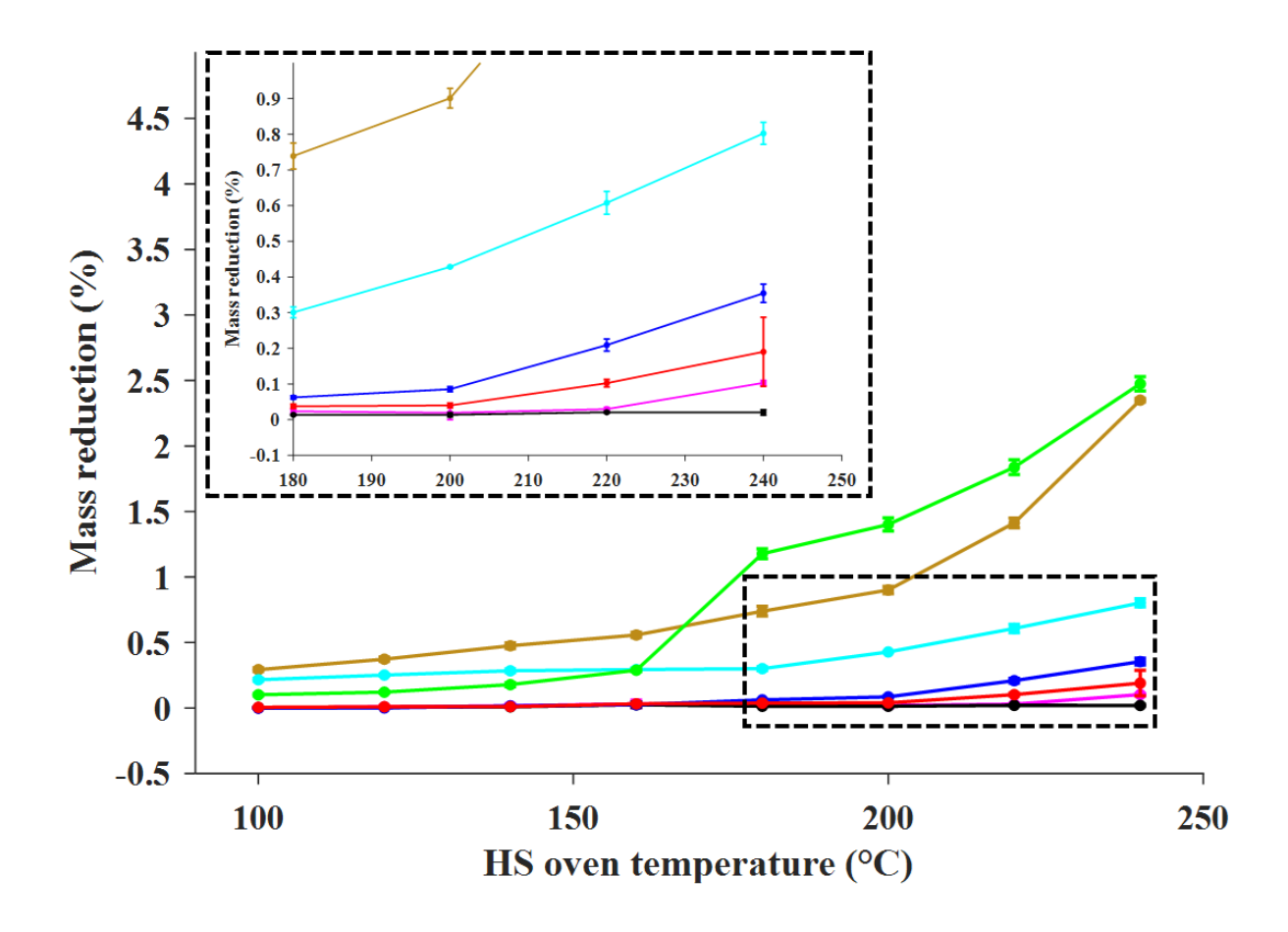


**Figure 1** Mass reduction of 3D printed models after they are subjected to headspace oven temperatures of 100 °C, 120 °C, 140 °C, 160 °C, 180 °C, 200 °C, 220 °C, and 240 °C for 20 mins. The mass of all models was taken before placing them into the 10 mL HS vials. All models were allowed to cool after heating and carefully removed from the vials to obtain the final mass. The green line represents SLA castable wax resin, brown line is SLA flexible 80A resin, light blue line represents SLA clear resin, dark blue line is the SLA high temperature resin, black line represents FDM polycarbonate (PC) filament, pink line represents FDM acrylonitrile butadiene styrene (ABS) filament, and red line represents FDM copolyester+ (CPE+) filament. The inset enlarges the response for HS oven temperatures ranging from 180 °C to 240 °C to allow better comparison of all materials in the high temperature zone.

the following order: castable wax > flexible 80A > clear > high temperature resin. The castable wax resin model exhibited an average mass reduction of 2.474 % with a standard deviation (STD) of  $\pm$  0.136 %, the flexible 80A resin exhibited an average mass reduction of 2.354 % (STD:  $\pm$  0.232 %), the clear resin exhibited an average mass reduction of 0.801 % (STD:  $\pm$  0.038 %), and

the high temperature resin exhibited an average mass reduction of 0.132 % (STD:  $\pm$  0.014 %). Percent relative standard deviation (RSD) values of 5.36%, 9.86 %, 4.79 %, and 11.76 %, respectively, were obtained for these models. Among all SLA materials, the high temperature resin exhibited the highest thermal stability and lowest mass loss at elevated temperatures.

At 240 °C, the mass reduction of FDM materials decreased in the following order: ABS > CPE+ > PC. ABS produced an average mass reduction of 0.364 % (STD:  $\pm 0.017$  %) and CPE+ exhibited an average mass reduction of 0.102 % (STD:  $\pm 0.014$  %). The RSD values for these two materials were 4.60 % and 12.31 %, respectively. The PC filament showed essentially no mass difference before and after a 20 minute incubation at 240 °C. Therefore, among all FDM materials, the PC filament showed the highest temperature stability by possessing the lowest mass reduction.

3.2 Examination of printing parameters on initial model mass and mass reduction for FDM materials

A number of printing parameters can be modified when using FDM 3D printers. These include increasing or decreasing the model's printing size either proportionally or non-proportionally on a 3-dimensional axis, adjusting the printcore temperature within a certain temperature range depending on the material, and varying the printing speed to enhance printing time efficiency. However, depending on the settings, the amount of filament extruded from the printcore can also vary which can directly affect the mass of the printed model. To investigate this in more detail, parameters including size of printed models, printing temperature, and printing speed were systematically varied and studied. Since the ABS filament exhibited the lowest thermal stability (i.e., highest mass reduction) among all FDM materials, it was used in subsequent sections as tuning its printing parameters would be expected to produce more obvious effects on mass reduction.

## 3.2.1 Influence of sample size

Printing dimension errors exist on all 3D printers regardless of the printing mechanism. However, due to differences in the design and actual print dimensions, a trial-and-error approach is commonly employed to obtain a more accurate dimension for final models. Because adjustments to the printing dimension are among the most important printing parameters, it was examined in this study. Printed models comprised of white ABS filament were printed as large (5 mm, 5 mm, 10 mm; L x W x H), medium (5 mm, 5 mm, 5 mm; L x W x H) and small (5 mm, 5 mm, 2.5 mm; L x W x H) sizes. As shown in Figure 2(a), the average mass of the large, medium, and small models were 0.7055 g (STD: ± 0.0016 g), 0.3692 g (STD: ± 0.0075 g), and 0.2027 g (STD: ± 0.0021 g), respectively, with RSD values of 0.02 %, 2.13 %, and 1.04 %.

Average mass reductions of the large, medium, and small models were 0.075 % (STD: 0.006 %), 0.036% (STD: 0.003%), and 0.023 % (STD: 0.003%), respectively, with RSD values of 8.46 %, 8.02 %, and 12.4 %. These results indicate that as the initial model mass increases, a larger mass reduction is measured. Dimension discrepancies between the setup in the modelling software and the actual printed model have been reported in previous studies using FDM (Akbaş *et al.*, 2020). Therefore, a trial-and-error approach is often applied to applications that require precise dimension control.

# 3.2.2 Effect of printcore temperature

Printcore temperature is a critical parameter that must be carefully optimized to obtain high-quality printed models. Ideally, a suitable range of printing temperatures for a specific material should be provided by the manufacturer. However, several factors such as the surrounding room temperature and the print bed temperature can affect the optimal printcore temperature.

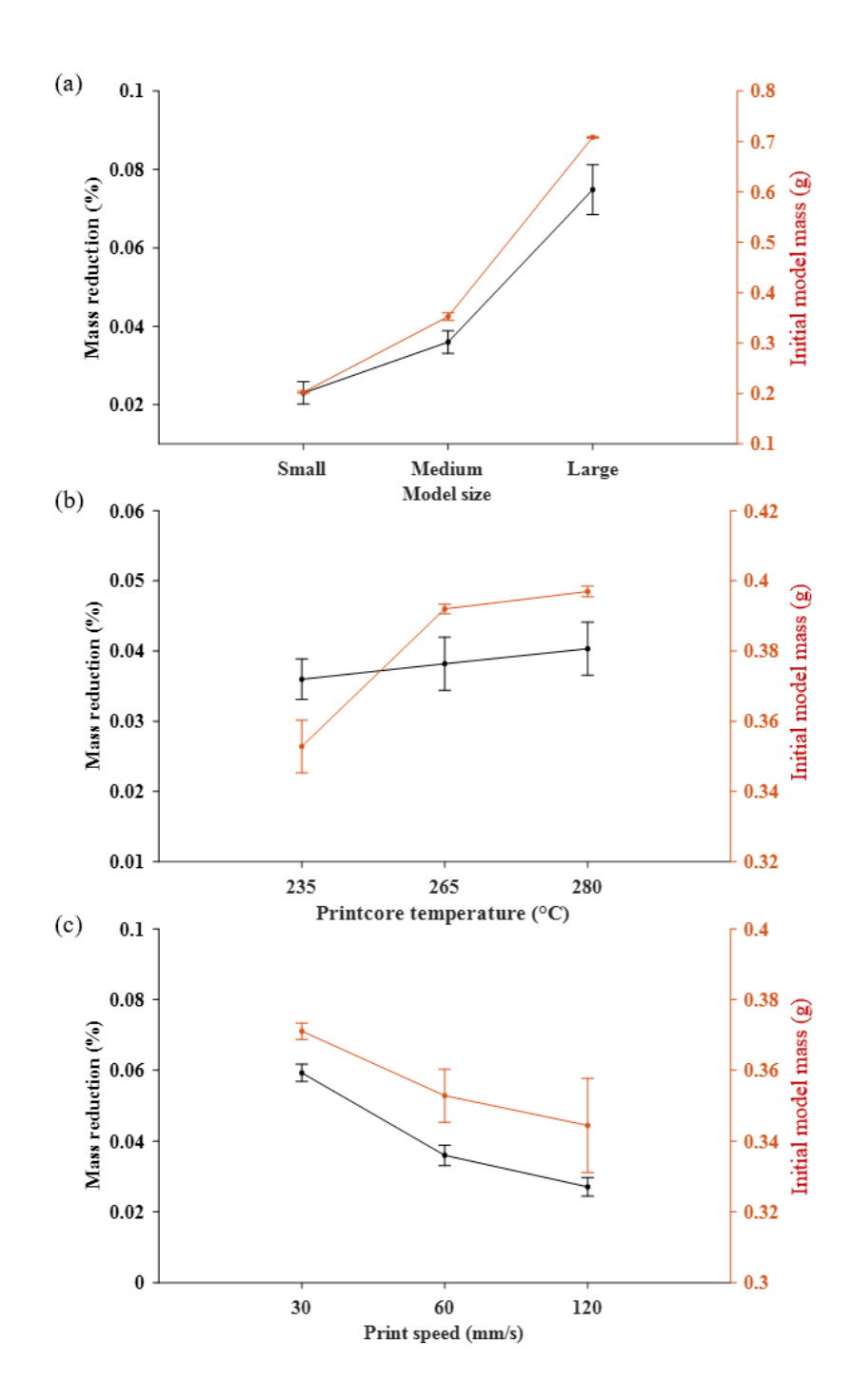


**Figure 2** Mass reduction as a function of (a) size (small, medium, large) of model, (b) printing temperature of 235 °C, 265 °C, 280 °C, and (c) printing speed of 30 mm/s, 60 mm/s, 120 mm/s printed using the ABS filament. Percentage of mass reduction was determined by placing models at a headspace oven temperature of 200 °C for 20 mins and calculated based on Equation 1. The black line represents the relation between percentage of mass reduction and the red line represents the relation between initial model mass by adjusting different setting parameters.

When the printcore temperature is set too low, filaments are not able to be smoothly extruded. Conversely, high printcore temperatures can lead to extra softness of the filament. Therefore, optimization of the printcore temperature is often needed and may influence the initial model mass. In this study, ABS filament was extruded at printcore temperatures of 235 °C (lowest suggested temperature), 265 °C (highest suggested temperature), and 280 °C (maximum printcore temperature). Triplicates of each printed model were incubated at 200 °C for 20 mins. As shown in Figure 2(b), the average masses of the printed models yielded the following order: 235 °C < 265 °C < 280 °C. Initial model masses of 0.3528 g (STD: ± 0.0075 g; RSD: 2.12 %), 0.3920 g (STD: ± 0.0013 g; RSD: 0.33 %), and 0.3970 g (STD: ± 0.0015 g; RSD: 0.38 %) were obtained when printing with printcore temperatures of 235 °C, 265 °C, and 280 °C, respectively. This demonstrates that high printcore temperatures result in more filament being extruded; however, extrusion of extra filament during high temperature printing can influence the smoothness of the model surface.

The average mass reductions of models printed at printcore temperatures of 235 °C, 265 °C, and 280 °C were 0.036 % (STD:  $\pm 0.0028$  %), 0.038 % (STD:  $\pm 0.0038$  %), and 0.040 % (STD:  $\pm 0.0038$  %), respectively. RSD values of 8.01 %, 9.93 %, and 9.38 %, respectively, were obtained from the corresponding printing temperature. This trend also agrees with the order obtained previously with the initial model mass in that the initial model mass is not significantly influenced by the printing temperature.

# 3.2.3 Analysis of printing speed

One of the main features distinguishing 3D printing from traditional manufacturing processes is the requirement of relatively short printing times. Increasing the printing speed can often shorten the overall printing time, resulting in time and energy savings. Since newly extruded

filaments require time to attach to the bottom layer, a fast moving nozzle may result in the model lacking form and structural integrity. Therefore, a compromise between the printing speed and printing time is often needed depending on the ultimate application.

In this study, models printed with white ABS filament extruded at a printing speed of 30 mm/s, 60 mm/s (default), and 120 mm/s were examined. Models were subjected to a HS oven temperature of 200 °C for 20 mins. Figure 2(c) shows that as the printing speed increased from 30 mm/s to 120 mm/s, the average initial model mass decreased in the following order: 30 mm/s > 60 mm/s > 120 mm/s. The average initial model masses yielded values of 0.3711 g (STD:  $\pm 0.0023 \text{ g}$ ), 0.3528 g (STD:  $\pm 0.0075 \text{ g}$ ), and 0.3440 g (STD:  $\pm 0.0133 \text{ g}$ ) while printing at speeds of 30 mm/s, 60 mm/s, and 120 mm/s, respectively, with RSD values of 0.62 %, 2.16 %, and 3.86 %. It can be expected that the faster moving extruders do not allow enough time for the filament to properly attach to the previous layers with less material being extruded.

Upon varying the printing speed, the average mass reduction decreased in the following order: 30 mm/s > 60 mm/s > 120 mm/s, with values of 0.0592 % (STD:  $\pm 0.0024 \%$ ), 0.0336 % (STD:  $\pm 0.0029 \%$ ), and 0.0272 % (STD:  $\pm 0.0026 \%$ ), respectively, and RSD values of 4.10 %, 8.01 %, and 9.76 %. These results are consistent with previously discussed results regarding printed mass and mass reduction.

## 3.3 Comparison of mass reduction for raw FDM filament and printed models

Thermal stabilities of raw ABS, CPE+, and PC filaments, as well as printed models produced from these filaments, were evaluated by examining the mass reduction at a HS oven temperature of 200 °C. The raw filaments were cut into several short 0.2-0.5 cm segments from the unprinted filament spool and then placed into headspace vials. Figure S2 shows a comparison

between the mass reduction of the FDM raw filaments and the models after their incubation at a HS oven temperature of 200 °C for 20 minutes. For all types of FDM materials, the mass reduction values of printed models are smaller than the raw filament. ABS models exhibited an average mass reduction of 0.0339 % (STD:  $\pm$  0.0075 %) whereas the raw filament produced an average mass reduction of 0.2662 % (STD:  $\pm$  0.012 %), with RSD values of 2.01 % and 4.75 %, respectively. CPE+ models showed an average mass reduction of 0.0617 % (STD:  $\pm$  0.0046 %) with the raw filament exhibiting an average mass reduction of 0.1542 % (STD:  $\pm$  0.010 %), with RSD values of 7.43 % and 6.34 %, respectively. The mass reduction of printed PC models was nearly negligible; however, the raw PC filament exhibited a mass reduction of 0.1139 % (STD:  $\pm$  0.0037 %) with a 3.26 % RSD. These results are to be expected since raw filaments are heated by the extruders once during the printing process to form the printed model and indicate that a significant amount of thermal degradation/decomposition products are released from the material during printing and varies depending on the material.

3.4 Effect of post-processing procedures on mass reduction for SLA materials under high temperature conditions

Unlike FDM, models printed by SLA involve an extensive post-processing procedure that typically consists of a solvent bath and further thermal and/or UV light curing processes to eliminate any uncured liquid resin. Standard post-processing procedures are often recommended by the manufacturer for each specific resin and improper post-processing procedures can lead to nonuniform structural composition or poor mechanical properties of the final models (Hardiman, 2019). In this study, the post-processing procedures were evaluated to observe their effects on the mass reduction of the final printed model. Two different post-processing modifications were

explored for the high temperature and flexible 80A resins and include eliminating both the washing/curing post-processing procedure and eliminating only the curing process using UV light.

Models obtained immediately after SLA printing are said be in a "green state" as their structure is more fragile and brittle than in their final form after UV curing (Hardiman, 2019). Due to their weaker material properties, green state models are usually treated with wet sand paper to smoothen the surface followed by further post-processing procedures to attain their optimal mechanical and thermal properties (Horvath and Cameron, 2020). The mass reduction of printed models was studied both in green state and after treatment with standard post-processing procedures, including washing and curing processes. Green state models printed by high temperature and flexible 80A resins were cleaned by lint-free wipes to remove any residual resin attached to the models. Standard post-processing procedures for each material were based on the manufacturers' suggestions prior to being subjected to a HS oven temperature of 200 °C for 20 mins.

As shown in Figure S3, models treated with the standard post-processing procedures exhibited less mass reduction than green state models after incubation at 200 °C. It can be expected that some thermal decomposition/degradation products may be released during the thermal curing process. As shown in Figure S3(a), mass reduction values of 0.7961 % (STD:  $\pm$  0.012 %) and 0.3007 % (STD:  $\pm$  0.015 %) were obtained for models subjected to standard post-processing procedures as well as models not subjected to the standard post-processing procedures, respectively, with RSD values of 1.55 % and 4.93 %.

The high temperature resin has been suggested by the manufacturer for use under elevated temperature applications; therefore, less mass reduction from the model is expected. As shown in Figure S3(b), nearly negligible mass reduction values of 0.0352 % (STD:  $\pm 0.0020 \%$ ) and 0.029

% (STD:  $\pm$  0.0016 %) were obtained for models with and without standard post-processing procedures, respectively. The results reveal that higher thermal stabilities of the models generally be obtained after they are treated with post-processing procedures.

UV light curing is an important step in the post-processing procedure as it enhances the thermal properties of the materials by further polymerizing trapped uncured resin layers in the models.(Cheah *et al.*, 1997) Although immersing the green state model into an IPA bath can remove uncured resin, unreacted layers confined in the cured polymer can ultimately lead to fragility of the models (Hardiman, 2019). Therefore, the recommended time and curing wavelength for UV light exposure is dependent on the type of material and is often provided by the manufacturer.

A comparison was made between models that were and were not exposed to UV light during post-processing procedures. As shown in Figure S4(a), models prepared from the flexible 80A resin that were not exposed to UV light experienced a mass reduction of 0.6064 % (STD: 0.0314 %, RSD: 4.92 %), whereas models subjected to a UV light curing step experienced a mass reduction of 0.3007 % (STD:  $\pm 0.0014$  %, RSD: 5.18 %). In the case of the high temperature resin shown in Figure S4(b), a trivial mass reduction of 0.0332 % (STD:  $\pm 0.0023$  %, RSD: 6.78 %) was obtained for models not exposed to UV light whereas models subjected to UV light curing experienced a mass reduction of 0.0292 % (STD:  $\pm 0.0016$  %, RSD: 5.53 %).

It has been discussed previously that the flexible 80A resin model produced a larger amount of thermal degradation/decomposition products than the high temperature resin after incubation under high temperature conditions. Due to its lower thermal stability, the flexible resin models exhibited a more significant mass reduction with respect to curing with/without UV light during the post-processing procedure. As expected, UV light treatment enhances the thermal stability of

the materials by further curing the resin that was not fully polymerized. Therefore, a lower mass reduction should be expected when treating models with UV light for all SLA materials.

# 3.5 Heat induced deformation of 3D printed models

FDM printing involves a melt extrusion method that requires thermoplastics as printing materials, which have been widely applied in injection molding within the manufacturing industry due to its softening property and tendency to become flexible at high temperatures (Miwa et al., 2017). Therefore, models printed by FDM can be expected to undergo some distortion. After SHS-GC-MS analysis, all models subjected to the various headspace oven temperatures were collected. As shown in Figure 3, FDM models exhibited signs of structural deformation, which may make them less desirable for users who require a model to maintain its structure within a high temperature environment. On the other hand, SLA printing results in the formation of thermoset polymers after polymerization of the resin. Thermoset polymers have been widely used in applications within the aerospace and automotive industry that require high dimensional stability. Due to molecular crosslinking, thermoset polymers form irreversible chemical bonds after exposure to UV light. The packed crosslinks also cause the thermoset polymer to not soften under high temperature and to retain a rigid structure or directly breakdown before reaching their melting temperature. As shown in Figure 3, SLA models remained structurally intact. However, discoloration can be observed from the transparent SLA models after incubation under high temperature conditions where they gradually became darker as the incubation temperature was increased.

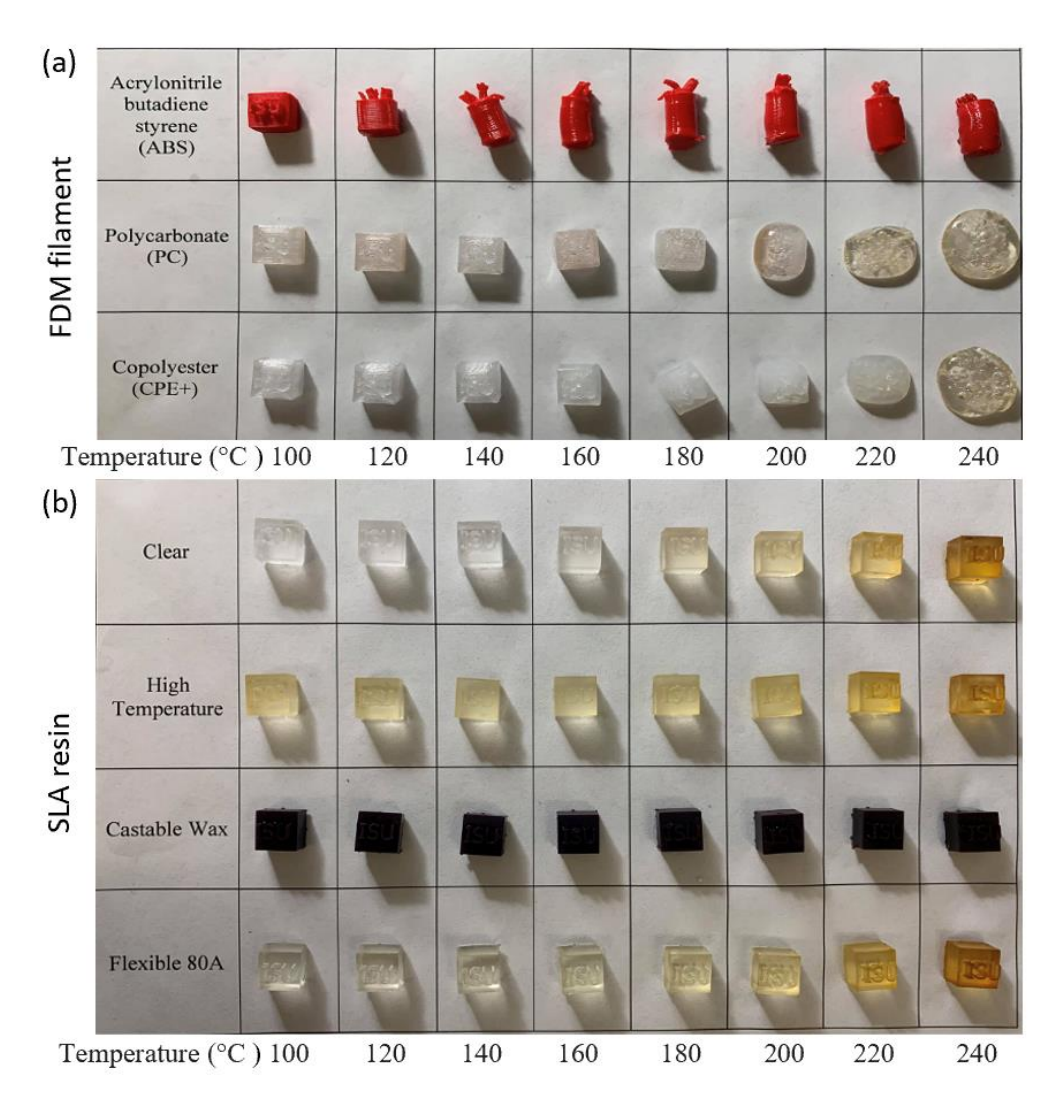


**Figure 3** Structural deformation of 3D printed models after being heated at a headspace oven temperature of 100 °C, 120 °C, 140 °C, 160 °C, 180 °C, 200 °C, 220 °C, 240 °C (from left to right) for 20 mins. The models include (a) FDM filaments (ABS, PC, CPE+) and (b) SLA resin (clear, high temperature, castable wax, flexible 80A).

## 3.6 Identification of thermal degradation products by SHS-GC-MS using high temperature resin

The proprietary nature of the various commercial 3D printing materials results in some ambiguity regarding their chemical composition. Commercial 3D printing materials often contain various additives such as monomers, crosslinkers, dyes, modifiers, plasticizers, and UV light stabilizers. Efforts have been undertaken to use various analytical methods to understand and

identify thermal decomposition/degradation products released during the printing process and from printed models when they are heated (Ding *et al.*, 2019; Rastogi *et al.*, 2020). In this study, SHS-GC-MS was applied to identify possible decomposition/degradation products due to its high sensitivity, accuracy, and high preconcentration of volatiles during sampling. The sensitivity of SHS-GC-MS is shown in Figure S5 using the PC filament, which has previously been shown to produce the lowest mass reduction of the models when incubated at 200 °C for 20 mins. While the mass reduction was nearly negligible from the previous method, several significant peaks can still be observed by using the SHS-GC-MS approach. Among all tested materials, the high temperature material exhibited high structural rigidity and relatively high temperature tolerance during thermal analysis. Therefore, this material was chosen to demonstrate the feasibility of SHS-GC-MS to identify small amounts of thermal decomposition/degradation products when the model is gradually heated.

To qualitatively evaluate thermal decomposition/degradation products in the high temperature resin, several high response peaks can be observed in the total ion GC chromatogram after the model was incubated at 200 °C, as shown in Figure 4. Among these peaks, a total of eight volatile compounds were identified as possible photoinitiators, monomers and crosslinkers by matching the obtained mass spectra with the NIST mass spectral library (de Almeida Monteiro Melo Ferraz *et al.*, 2020; Ziolli and Jardim, 2003). Figure S6(a) and (b) show the alignment of the mass spectra obtained from the high temperature resin during SHS-GC-MS and from the database. The peaks were found to align with at least an 80 % match to the mass spectra from the database and are shown in Table 1. Commercial standards of these compounds were purchased and subjected to GC-MS analysis allowing for the retention times of the commercial standards to be matched with compounds identified from the library search. Retention times of the identified

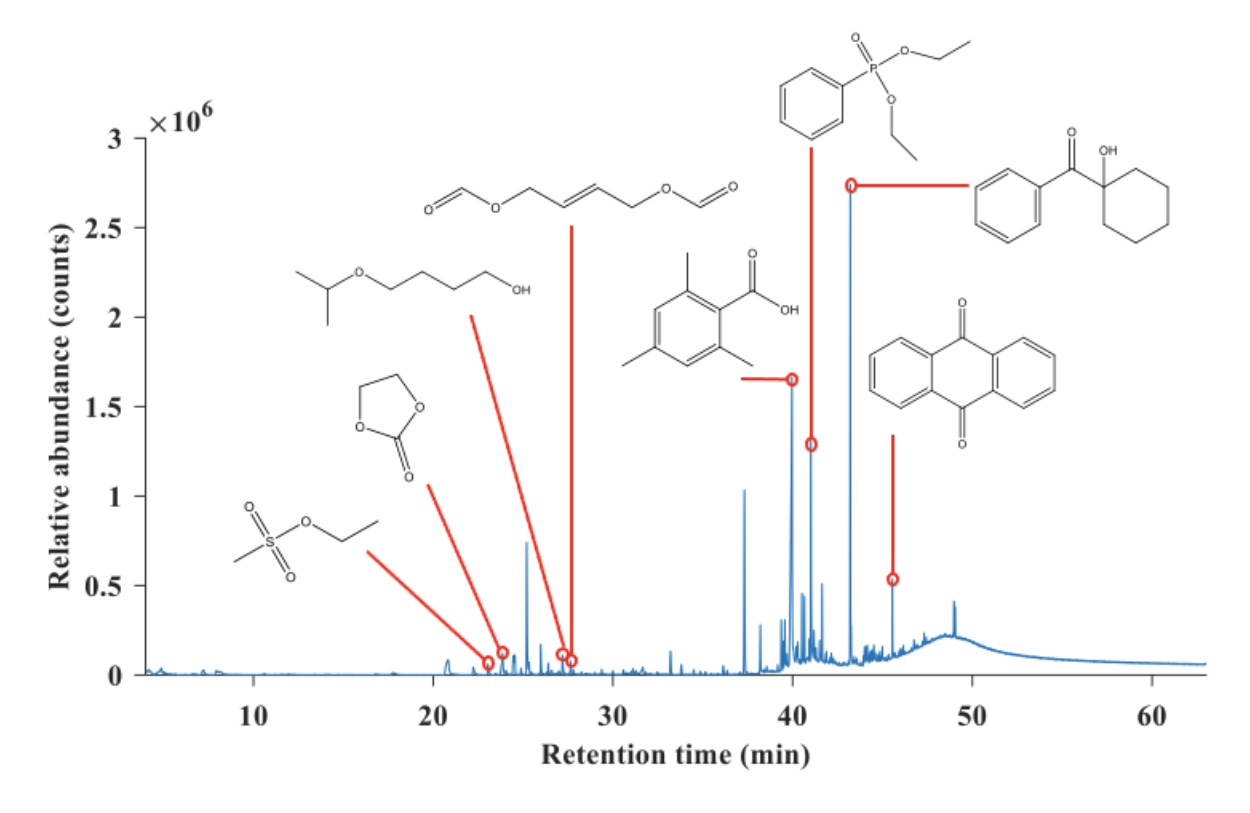


**Figure 4** GC-MS total ion chromatogram of the high temperature resin obtained after incubating the sample at a headspace oven temperature of 200 °C for 20 mins. Chemical structures are noted for peaks with probabilities over 80 % by matching the obtained mass spectra of the compounds with the NIST mass spectral library.

compounds generally matched the standard within 0.1 minutes due to the length of the transferline between the SHS sampler and GC-MS system. As shown in Figure 4, ethyl methanesulfonate extracted from the 3D printed model exhibited a retention time of 23.0 minutes, whereas the ethyl methanesulfonate standard produced a retention time of 22.9 minutes. A 96.2 % probability of peak alignment matched the mass spectrum obtained from the NIST mass spectral library. The analyte 1,3-dioxolan-2-one exhibited a retention time of 24.5 minutes and has been reported as a commonly used monomer for UV light polymerization reactions by undergoing a ring opening reaction (Xu *et al.*, 2019). The retention time of the commercial standard was 24.4 minutes with a 93.3 % match to the NIST mass spectral library. The compound 4-propan-2-yloxybutan-1-ol

**Table I.** Identification of unknown compounds from thermal degradation of the high temperature resin model (SLA) after incubation at a HS oven of 200 °C for 20 mins. Retention times of thermal degradation compounds were acquired from analytes that underwent degradation from the 3D printed model and were injected by the SHS sampler. Retention times of commercial standard were acquired by direct injection. Probabilities are acquired by matching peaks between the mass spectrum obtained from the thermal degradation/decomposition products and the mass spectrum from the NIST mass spectral library.

Compound name <sup>a</sup>	Chemical formula <sup>a</sup>	Retention time of thermal degradation/de composition product <sup>b</sup> (min)	Retention time of commercial standard <sup>b</sup> (min)	Observed base peak <sup>a</sup> (m/z)	Probability <sup>a</sup> (%)
Ethyl methanesulfonate	C <sub>3</sub> H <sub>8</sub> O <sub>3</sub> S	23.0	22.9	79	96.2
1,3-Dioxolan-2-one	C <sub>3</sub> H <sub>4</sub> O <sub>3</sub>	24.5	24.4	88	93.3
4-Propan-2- yloxybutan-1-ol	C <sub>7</sub> H <sub>16</sub> O <sub>2</sub>	27.1	N/A	45	82.3
[( <i>E</i> )-4-Formyloxybut- 2-enyl] formate	$C_6H_8O_4$	27.8	N/A	54	95.4
2,4,6-Trimethylbenzoic acid	C <sub>10</sub> H <sub>12</sub> O <sub>2</sub>	39.9	39.9	146	81.9
Diethoxyphosphorylbe nzene	$C_{10}H_{15}O_3P$	41.0	41.0	158	96.4
(1- Hydroxycyclohexyl)- phenylmethanone	C <sub>13</sub> H <sub>16</sub> O <sub>2</sub>	43.2	43.2	99	93.3
Anthracene-9,10-dione	$C_{14}H_8O_2$	45.5	45.5	208	82.7

<sup>&</sup>lt;sup>a</sup> Data acquired from the Agilent Mass Hunter software.

extracted from the 3D printed model exhibited a retention time of 27.1 minutes and a 82.3 % probability match. The analyte [(E)-4-Formyloxybut-2-enyl] formate produced a retention time of 27.8 minutes, and a 95.4 % match to the mass spectrum from the NIST mass spectral library. The compound 2,4,6-trimethylbenzoic acid was identified at a retention time of 39.9 minutes and is a common photodecomposition product from UV photoinitiators after polymerization (Scarsella et

<sup>&</sup>lt;sup>b</sup> Data obtained from National Institute of Standards and Technology (NIST) mass spectral library. N/A: No commercial standard available.

al., 2019). The retention time of the 2,4,6-trimethylbenzoic acid standard was 39.9 minutes with a 81.9 % probability of mass spectrum peak alignment with the NIST mass spectral library. The compound 1-hydroxycyclohexylphenyl ketone is a common UV light photoinitiator used in resinbased additive manufacturing industry (Cheah et al., 1997). A 93.3 % of probability was obtained for this compound by alignment to the mass spectrum of the NIST database. Finally, the compound 9,10-anthracenedione is commonly used with an amine co-initiator to perform a type-2 photoinitiation (Dadashi-Silab et al., 2016). Retention times obtained from both the 3D printed model and the standard were found at 45.5 minutes with an 82.7 % probability by alignment to the mass spectrum from the NIST mass spectral library.

## 4. Conclusions

This study demonstrates SHS-GC-MS as a simple and sensitive preconcentration method to analyze thermal degradation products produced from 3D printed models under high temperature conditions. The use of the SHS-GC-MS approach enables precise temperature control with the SHS oven to enable emission and preconcentration of thermal degradation products from the 3D printed models and identification of these compounds from chromatographic retention times and mass spectra. The mass loss of models in relation to adjustments of FDM printing parameters (size, printcore temperature and printing speed) and SLA printing post-processing processing procedures on the tested material was measured in this study. The mass loss was found to increase as larger sample sizes and faster printing speeds were set for FDM printing whereas the mass loss increased without proper treatment of SLA 3D printed models. In addition, deformation of the models was also found to be dependent on different 3D printing mechanisms under various incubation temperatures. While FDM printed models tended to deform under high temperature, SLA printed model remain structurally intact even after incubation at 240 °C. Lastly, the identification of the

thermal degradation produced from 3D printed models under high temperatures was enabled by mass spectral alignments. Using the high temperature resin, mass spectra of thermal degradation compounds emitted from the high temperature model were aligned to the standard mass spectra from the NIST mass spectral library. The SHS-GC-MS approach holds great potential in identifying thermal degradation compounds emitted from commercial 3D printing materials with unknown composition.

## Acknowledgements

J.L.A. acknowledges funding from the Chemical Measurement and Imaging Program at the National Science Foundation (Grant No. CHE-1709372). J.L.A. and S-A.H. acknowledge the Alice Hudson Professorship for support.

**Compliance with ethical standards**. This article conforms to all ethical standards.

**Conflicts of interest.** The authors declare no conflicts of interest.

#### References

- Akbaş, O. E., Hıra, O., Hervan, S. Z., Samankan, S.and Altınkaynak, A. (2020), "Dimensional accuracy of FDM-printed polymer parts." *Rapid Prototyping Journal*, Vol. 26, pp. 288-298.
- Alvarado, J. S.and Rose, C. (2004), "Static headspace analysis of volatile organic compounds in soil and vegetation samples for site characterization." *Talanta*, Vol. 62, pp. 17-23.
- Au, A. K., Huynh, W., Horowitz, L. F.and Folch, A. (2016), "3D-Printed Microfluidics." *Angewandte Chemie International Edition*, Vol. 55, pp. 3862-3881.
- Awad, A., Fina, F., Goyanes, A., Gaisford, S.and Basit, A. W. (2020), "3D printing: Principles and pharmaceutical applications of selective laser sintering." *International Journal of Pharmaceutics*, Vol. 586, pp. 119594.
- Badaro, J. P. M., Campos, V. P., Da Rocha, F. O. C.and Santos, C. L. (2021), "Multivariate analysis of the distribution and formation of trihalomethanes in treated water for human consumption." *Food Chem*, Vol. 365, pp. 130469.
- Basak, I., Nowicki, G., Ruttens, B., Desta, D., Prooth, J., Jose, M., Nagels, S., Boyen, H. G., D'haen, J., Buntinx, M.and Deferme, W. (2020), "Inkjet Printing of PEDOT:PSS Based Conductive Patterns for 3D Forming Applications." *Polymers (Basel)*, Vol. 12.

- Bernatikova, S., Dudacek, A., Prichystalova, R., Klecka, V.and Kocurkova, L. (2021), "Characterization of Ultrafine Particles and VOCs Emitted from a 3D Printer." *Int J Environ Res Public Health*, Vol. 18.
- Blok, L. G., Longana, M. L., Yu, H. and Woods, B. K. S. (2018), "An investigation into 3D printing of fibre reinforced thermoplastic composites." *Additive Manufacturing*, Vol. 22, pp. 176-186.
- Borrello, J., Nasser, P., Iatridis, J. C.and Costa, K. D. (2018), "3D printing a mechanically-tunable acrylate resin on a commercial DLP-SLA printer." *Additive Manufacturing*, Vol. 23, pp. 374-380.
- Campbell, I., Bourell, D.and Gibson, I. (2012), "Additive manufacturing: rapid prototyping comes of age." *Rapid Prototyping Journal*, Vol. 18, pp. 255-258.
- Cardador, M. J.and Gallego, M. (2017), "Simultaneous determination of 14 disinfection by-products in meat products using microwave-assisted extraction and static headspace coupled to gas chromatography-mass spectrometry." *J Chromatogr A*, Vol. 1509, pp. 9-15.
- Carvalho, J., Puertas, G., Gaspar, J., Azinheiro, S., Dieguez, L., Garrido-Maestu, A., Vazquez, M., Barros-Velazquez, J., Cardoso, S.and Prado, M. (2018), "Highly efficient DNA extraction and purification from olive oil on a washable and reusable miniaturized device." *Anal Chim Acta*, Vol. 1020, pp. 30-40.
- Chan, F. L., Hon, C. Y., Tarlo, S. M., Rajaram, N.and House, R. (2020), "Emissions and health risks from the use of 3D printers in an occupational setting." *J Toxicol Environ Health A*, Vol. 83, pp. 279-287.
- Chan, K., Coen, M., Hardick, J., Gaydos, C. A., Wong, K. Y., Smith, C., Wilson, S. A., Vayugundla, S. P.and Wong, S. (2016), "Low-Cost 3D Printers Enable High-Quality and Automated Sample Preparation and Molecular Detection." *PLoS One*, Vol. 11, pp. e0158502.
- Cheah, C. M., Fuh, J. Y. H., Nee, A. Y. C., Lu, L., Choo, Y. S.and Miyazawa, T. (1997), "Characteristics of photopolymeric material used in rapid prototypes Part II. Mechanical properties at post-cured state." *Journal of Materials Processing Technology*, Vol. 67, pp. 46-49.
- Choong, Y. Y. C., Tan, H. W., Patel, D. C., Choong, W. T. N., Chen, C.-H., Low, H. Y., Tan, M. J., Patel, C. D.and Chua, C. K. (2020), "The global rise of 3D printing during the COVID-19 pandemic." *Nature Reviews Materials*, Vol. 5, pp. 637-639.
- Dadashi-Silab, S., Doran, S.and Yagci, Y. (2016), "Photoinduced Electron Transfer Reactions for Macromolecular Syntheses." *Chemical Reviews*, Vol. 116, pp. 10212-10275.
- De Almeida Monteiro Melo Ferraz, M., Nagashima, J. B., Venzac, B., Le Gac, S.and Songsasen, N. (2020), "3D printed mold leachates in PDMS microfluidic devices." *Scientific Reports*, Vol. 10, pp. 994.
- Ding, S., Ng, B. F., Shang, X., Liu, H., Lu, X.and Wan, M. P. (2019), "The characteristics and formation mechanisms of emissions from thermal decomposition of 3D printer polymer filaments." *Science of The Total Environment*, Vol. 692, pp. 984-994.
- Even, M., Girard, M., Rich, A., Hutzler, C.and Luch, A. (2019), "Emissions of VOCs From Polymer-Based Consumer Products: From Emission Data of Real Samples to the Assessment of Inhalation Exposure." *Front Public Health*, Vol. 7, pp. 202.
- Ford, S.and Minshall, T. (2019), "Invited review article: Where and how 3D printing is used in teaching and education." *Additive Manufacturing*, Vol. 25, pp. 131-150.

- Fuller, J., White, D., Yi, H., Colley, J., Vickery, Z.and Liu, S. (2020), "Analysis of volatile compounds causing undesirable odors in a polypropylene high-density polyethylene recycled plastic resin with solid-phase microextraction." *Chemosphere*, Vol. 260, pp. 127589.
- Guerra, A. J., Lammel-Lindemann, J., Katko, A., Kleinfehn, A., Rodriguez, C. A., Catalani, L. H., Becker, M. L., Ciurana, J.and Dean, D. (2019), "Optimization of photocrosslinkable resin components and 3D printing process parameters." *Acta Biomaterialia*, Vol. 97, pp. 154-161.
- Hardiman, K. (2019), Post-processing Considerations for Biomedical 3D Printing of Polymers. *In:* DEVINE, D. M. (Ed.) *Polymer-Based Additive Manufacturing: Biomedical Applications*. Cham: Springer International Publishing.
- Hearn, M. T. W. (2017), "Trends in additive manufacturing of chromatographic and membrane materials." *Current Opinion in Chemical Engineering*, Vol. 18, pp. 90-98.
- Hong, J. K., Kim, S. K., Heo, S. J. and Koak, J. Y. (2020), "Mechanical Properties and Metal-Ceramic Bond Strength of Co-Cr Alloy Manufactured by Selective Laser Melting." *Materials (Basel)*, Vol. 13.
- Horvath, J. and Cameron, R. (2020), Surface Finishing Filament Prints. *In:* HORVATH, J. & CAMERON, R. (Ed.s.) *Mastering 3D Printing: A Guide to Modeling, Printing, and Prototyping.* Berkeley, CA: Apress.
- Kahl, M., Gertig, M., Hoyer, P., Friedrich, O.and Gilbert, D. F. (2019), "Ultra-Low-Cost 3D Bioprinting: Modification and Application of an Off-the-Shelf Desktop 3D-Printer for Biofabrication." *Frontiers in bioengineering and biotechnology*, Vol. 7, pp. 184-184.
- Kalsoom, U., Nesterenko, P. N. and Paull, B. (2018), "Current and future impact of 3D printing on the separation sciences." *TrAC Trends in Analytical Chemistry*, Vol. 105, pp. 492-502.
- Li, F., Ceballos, M. R., Balavandy, S. K., Fan, J., Khataei, M. M., Yamini, Y.and Maya, F. (2020), "3D Printing in analytical sample preparation." *J Sep Sci*, Vol. 43, pp. 1854-1866.
- Macdonald, E., Salas, R., Espalin, D., Perez, M., Aguilera, E., Muse, D.and Wicker, R. B. (2014), "3D Printing for the Rapid Prototyping of Structural Electronics." *IEEE Access*, Vol. 2, pp. 234-242.
- Miwa, T., Kitagawa, D., Nagatsuka, K., Yamaoka, H., Ito, K.and Nakata, K. (2017), "Dissimilar materials joining between stainless steel and carbon fiber reinforced thermoplastic by friction lap joining." *Quarterly Journal of The Japan Welding Society*, Vol. 35, pp. 29-35.
- Moseng, B. (1992), "Desk Top Manufacturing Using Stereolithography (Sla) Techniques." *Ifip Transactions B-Applications in Technology*, Vol. 1, pp. 323-332.
- Mwema, F. M.and Akinlabi, E. T. (2020), Basics of Fused Deposition Modelling (FDM). *Fused Deposition Modeling*.
- Potter, P. M., Al-Abed, S. R., Lay, D.and Lomnicki, S. M. (2019), "VOC Emissions and Formation Mechanisms from Carbon Nanotube Composites during 3D Printing." *Environmental Science & Technology*, Vol. 53, pp. 4364-4370.
- Rastogi, P., Gharde, S.and Kandasubramanian, B. (2020), Thermal Effects in 3D Printed Parts. *In:* SINGH, S., PRAKASH, C. & SINGH, R. (Ed.s.) *3D Printing in Biomedical Engineering.* Singapore: Springer Singapore.
- Rayna, T.and Striukova, L. (2016), "From rapid prototyping to home fabrication: How 3D printing is changing business model innovation." *Technological Forecasting and Social Change*, Vol. 102, pp. 214-224.

- Rodinkov, O. V., Bugaichenko, A. S. and Moskvin, L. N. (2020), "Static Headspace Analysis and Its Current Status." *Journal of Analytical Chemistry*, Vol. 75, pp. 1-17.
- Russo, M. V., Notardonato, I., Rosada, A., Ianiri, G.and Avino, P. (2021), "Halogenated Volatile Organic Compounds in Water Samples and Inorganic Elements Levels in Ores for Characterizing a High Anthropogenic Polluted Area in the Northern Latium Region (Italy)." *Int J Environ Res Public Health*, Vol. 18.
- Scarsella, J. B., Zhang, N.and Hartman, T. G. (2019), "Identification and Migration Studies of Photolytic Decomposition Products of UV-Photoinitiators in Food Packaging." *Molecules (Basel, Switzerland)*, Vol. 24, pp. 3592.
- Srinivasan, R., Giannikas, V., Mcfarlane, D.and Ahmed, M. (2017), Customisation in Manufacturing: The Use of 3D Printing. *Service Orientation in Holonic and Multi-Agent Manufacturing*.
- Stephens, B., Azimi, P., El Orch, Z.and Ramos, T. (2013), "Ultrafine particle emissions from desktop 3D printers." *Atmospheric Environment*, Vol. 79, pp. 334-339.
- Su, C. K., Peng, P. J.and Sun, Y. C. (2015), "Fully 3D-Printed Preconcentrator for Selective Extraction of Trace Elements in Seawater." *Analytical Chemistry*, Vol. 87, pp. 6945-50.
- Valino, A. D., Dizon, J. R. C., Espera, A. H., Chen, Q., Messman, J. and Advincula, R. C. (2019), "Advances in 3D printing of thermoplastic polymer composites and nanocomposites." *Progress in Polymer Science*, Vol. 98, pp. 101162.
- Wang, C., Zhong, W., Ping, W., Lin, Z., Wang, R., Dai, J., Guo, M., Xiong, W., Zhao, J. C.and Hu, L. (2021), "Rapid Synthesis and Sintering of Metals from Powders." *Adv Sci (Weinh)*, Vol. 8, pp. e2004229.
- Wang, L.and Pumera, M. (2021), "Recent advances of 3D printing in analytical chemistry: Focus on microfluidic, separation, and extraction devices." *TrAC Trends in Analytical Chemistry*, Vol. 135, pp. 116151.
- Warr, C., Valdoz, J. C., Bickham, B. P., Knight, C. J., Franks, N. A., Chartrand, N., Van Ry, P. M., Christensen, K. A., Nordin, G. P.and Cook, A. D. (2020), "Biocompatible PEGDA Resin for 3D Printing." *ACS Applied Bio Materials*, Vol. 3, pp. 2239-2244.
- Weigel, N., Mannel, M. J.and Thiele, J. (2021), "Flexible Materials for High-Resolution 3D Printing of Microfluidic Devices with Integrated Droplet Size Regulation." *ACS Appl Mater Interfaces*, Vol. 13, pp. 31086-31101.
- Weisgrab, G., Ovsianikov, A.and Costa, P. F. (2019), "Functional 3D Printing for Microfluidic Chips." *Advanced Materials Technologies*, Vol. 4, pp. 1900275.
- Xu, Y., Perry, M. R., Cairns, S. A.and Shaver, M. P. (2019), "Understanding the ring-opening polymerisation of dioxolanones." *Polymer Chemistry*, Vol. 10, pp. 3048-3054.
- Yarramraju, S., Akurathi, V., Wolfs, K., Van Schepdael, A., Hoogmartens, J. and Adams, E. (2007), "Investigation of sorbic acid volatile degradation products in pharmaceutical formulations using static headspace gas chromatography." *J Pharm Biomed Anal*, Vol. 44, pp. 456-63.
- Zhang, Q., Pardo, M., Rudich, Y., Kaplan-Ashiri, I., Wong, J. P. S., Davis, A. Y., Black, M. S.and Weber, R. J. (2019), "Chemical Composition and Toxicity of Particles Emitted from a Consumer-Level 3D Printer Using Various Materials." *Environmental Science & Technology*, Vol. 53, pp. 12054-12061.
- Ziolli, R. L.and Jardim, W. F. (2003), "Photochemical transformations of water-soluble fraction (WSF) of crude oil in marine waters: A comparison between photolysis and accelerated degradation with TiO2 using GC–MS and UVF." *Journal of Photochemistry and Photobiology A: Chemistry*, Vol. 155, pp. 243-252.